

# Production of a chiral magnetic anomaly with emerging turbulence and mean-field dynamo action

Jennifer Schober,<sup>1,\*</sup> Igor Rogachevskii,<sup>2,3</sup> and Axel Brandenburg<sup>3,4,5,6</sup>

<sup>1</sup>*Laboratoire d'Astrophysique, EPFL, CH-1290 Sauverny, Switzerland*

<sup>2</sup>*Department of Mechanical Engineering, Ben-Gurion University of the Negev, P.O. Box 653, Beer-Sheva 84105, Israel*

<sup>3</sup>*Nordita, KTH Royal Institute of Technology and Stockholm University, 10691 Stockholm, Sweden*

<sup>4</sup>*Department of Astronomy, AlbaNova University Center, Stockholm University, 10691 Stockholm, Sweden*

<sup>5</sup>*School of Natural Sciences and Medicine, Iliia State University, 0194 Tbilisi, Georgia*

<sup>6</sup>*McWilliams Center for Cosmology and Department of Physics, Carnegie Mellon University, Pittsburgh, PA 15213, USA*

(Dated: July 28, 2021)

In relativistic magnetized plasmas, asymmetry in the number densities of left- and right-handed fermions, i.e., a non-zero chiral chemical potential  $\mu_5$ , leads to an electric current along the magnetic field. This causes a chiral dynamo instability for a uniform  $\mu_5$ , but our simulations reveal dynamos even for fluctuating  $\mu_5$  with zero mean. This generates small-scale magnetic helicity and turbulence. A large-scale  $\mu_5$  emerges due to chirality conservation. These effects amplify a mean magnetic field via the magnetic  $\alpha$  effect and produce a universal scale-invariant  $\mu_5$  spectrum.

The chiral magnetic effect (CME) is a macroscopic quantum phenomenon and follows from the chiral anomaly in quantum field theory. It describes the occurrence of an electric current along an external magnetic field in the presence of an asymmetry between the number densities of left- and right-handed electrically charged fermions [1]. This is a direct consequence of the coupling of fermionic chirality and the topology of magnetic field lines characterized by magnetic helicity [2, 3]. Chiral asymmetry is by quantified the chiral chemical potential  $\mu_5 \equiv \mu_L - \mu_R$ , which is nonzero in spatial regions where the chemical potentials of left-handed ( $\mu_L$ ) and right-handed ( $\mu_R$ ) chiral fermions differ from one another. It has been shown [4] that  $\mu_5$  can survive down to energies of  $\approx 10$  MeV and thereby the CME can potentially affect leptogenesis during the QCD phase transition [5] and produce gravitational waves in the early Universe [6].

The dynamics of a chiral fluid has been studied using different approaches [4, 7, 8] including kinetic theory [9–12]. Yet the additional electric current related to the CME can also be included in an effective description of a chiral plasma, so-called chiral magnetohydrodynamics (MHD) [13–16]. The coupling between  $\mu_5$  and magnetic helicity in chiral MHD leads to new dynamics of the system compared to classical MHD. The CME can induce a dynamo instability in the magnetic field on small length scales [17]. Unlike classical MHD dynamos, chiral dynamos can occur without an initial velocity field, leading to a self-consistent production of velocity fluctuations through the Lorentz force. Subsequent production of turbulence and the occurrence of a chiral mean-field dynamo have been proposed [14] and confirmed by direct numerical simulations (DNS) [18–20].

The possibility of efficient magnetic field amplification through the CME has relevance for the physics of the early Universe. In particular, the transport of magnetic energy to large length scales via a chiral inverse cascade

[4, 21, 22] or amplification on large scales through the chiral mean-field dynamo, strongly increases the chance of primordial magnetic fields [23, 24] to survive until present day. Thereby, observational constraints on magnetic fields in cosmic voids [25] may open up a unique window into the fundamental physics of the early Universe. Beyond cosmology, chiral MHD has also relevance to neutron stars [26–31], quark-gluon plasmas in heavy-ion collisions [2, 3, 32], and quantum materials [33].

In all previous chiral dynamo studies, a uniform initial  $\mu_5$  has been considered [14, 18–20]. However, the origin of a uniform  $\mu_5$  is not entirely clear and requires special generation mechanisms. In this Letter, we consider a more general and universal situation with initial fluctuations of the chiral chemical potential with zero mean.

For the analysis, we normalize  $\mu_5$  by  $4\alpha_{\text{em}}/(\hbar c)$  such that it has the dimension of inverse length, where  $\alpha_{\text{em}} \approx 1/137$  is the fine structure constant,  $c$  is the speed of light, and  $\hbar$  is the reduced Planck constant. The strength of the coupling of the electromagnetic field to  $\mu_5$  is characterized by the chiral feedback parameter  $\lambda$  which, for hot plasmas,  $k_B T \gg \max(|\mu_L|, |\mu_R|)$ , is given by  $\lambda = 3\hbar c(8\alpha_{\text{em}})^2/(k_B T)^2$ , where  $T$  is the temperature and  $k_B$  is the Boltzmann constant. We consider the following set of chiral MHD equations:

$$\frac{\partial \mathbf{B}}{\partial t} = \nabla \times [\mathbf{U} \times \mathbf{B} - \eta (\nabla \times \mathbf{B} - \mu_5 \mathbf{B})], \quad (1)$$

$$\rho \frac{D\mathbf{U}}{Dt} = (\nabla \times \mathbf{B}) \times \mathbf{B} - \nabla p + \nabla \cdot (2\nu \rho \mathbf{S}), \quad (2)$$

$$\frac{D\rho}{Dt} = -\rho \nabla \cdot \mathbf{U}, \quad (3)$$

$$\frac{D\mu_5}{Dt} = \mathcal{D}_5(\mu_5) + \lambda \eta [\mathbf{B} \cdot (\nabla \times \mathbf{B}) - \mu_5 \mathbf{B}^2], \quad (4)$$

where the magnetic field  $\mathbf{B}$  is normalized such that the magnetic energy density is  $\mathbf{B}^2/2$ , and the advective derivative is  $D/Dt = \partial/\partial t + \mathbf{U} \cdot \nabla$  with  $\mathbf{U}$  being the

velocity field. Further,  $\eta$  is the microscopic magnetic diffusivity,  $p$  is the fluid pressure,  $S_{ij} = (U_{i,j} + U_{j,i})/2 - \delta_{ij}(\nabla \cdot \mathbf{U})/3$  are the components of the trace-free strain tensor  $\mathbf{S}$  (commas denote partial spatial derivatives) and  $\nu$  is the kinematic viscosity. We adopt an isothermal equation of state,  $p = \rho c_s^2$ , with  $c_s$  being the sound speed.

In Eqs. (1)–(4), we do not include the evolution equation for the chemical potential. It allows to describe chiral magnetic waves [34] for an equilibrium magnetic field. On the other hand, here we study various dynamos excited from a very small seed magnetic field. Equations (1)–(4) imply that total chirality  $\chi_{\text{tot}} \equiv \langle \mathcal{H} \rangle + 2\langle \mu_5 \rangle / \lambda$  is conserved, where angle brackets denote volume averaging. Here,  $\langle \mathcal{H} \rangle \equiv \langle \mathbf{A} \cdot \mathbf{B} \rangle$  is magnetic helicity with  $\mathbf{B} = \nabla \times \mathbf{A}$  being the magnetic field and  $\mathbf{A}$  is the vector potential.

At the initial time  $t_0$ , we assume  $\langle \mu_5 \rangle(t_0) = 0$ , but non-zero fluctuations  $\mu_5'$  of the chiral chemical potential,  $\langle \mu_5'^2 \rangle(t_0) \neq 0$ . At the initial time, small fluctuations of  $\mathbf{B}$  with zero mean are present, while the velocity field is assumed to be zero. Fluctuations of  $\mu_5'$  result in an exponential growth of the magnetic field strength due to the chiral dynamo. This instability is caused by the term  $\nabla \times (v_5 \mathbf{B})$  in Eq. (1) with  $v_5 = \eta \mu_5$  and has a growth rate  $\gamma(k) = |v_5|k - \eta k^2$ , with  $k$  being the wave number [17]. Owing to a term  $\propto v_5$  in the governing dispersion relation, this instability is referred to as  $v_5$  dynamo, which occurs when  $|v_5| > \eta k$  or, alternatively,  $|\mu_5| > \min(k)$ . The maximum growth rate of this instability is  $\gamma_5 = v_5^2/4\eta$ , which is attained at wave number  $k_5 = |\mu_5|/2$ . We note that, while the  $\nabla \times (v_5 \mathbf{B})$  term in Eq. (1) is formally similar to the  $\alpha$  effect in classical mean-field MHD [14], the velocity  $v_5$  is not produced by helical turbulence, but rather by the CME which is a quantum effect. During the  $v_5$  dynamo phase, magnetic fluctuations produce velocity fluctuations via the Lorentz force  $(\nabla \times \mathbf{B}) \times \mathbf{B}$ , in Eq. (2).

Since the initial mean chiral chemical potential is zero, and the initial small-scale magnetic helicity  $\langle \mathbf{a} \cdot \mathbf{b} \rangle(t_0)$  related to the fluctuations of the vector potential  $\mathbf{a}$  and the magnetic field  $\mathbf{b}$  vanishes, we have  $\chi_{\text{tot}}(t_0) = 0$ . Due to the conservation of total chirality, it stays zero at all times:  $\chi_{\text{tot}}(t) = 0$ . Initial fluctuations of a chiral chemical potential  $\mu_5'$  with a wide range of scales produce  $\mathbf{b}$  by the  $v_5$  dynamo. Indeed, for a wide spectrum in  $k$  space, fluctuations of  $\mu_5$  on larger scales serve as a *mean field* for fluctuations on smaller scales, so that the chiral dynamo instability excites magnetic fluctuations at small scales and produces small-scale magnetic helicity  $\langle \mathbf{a} \cdot \mathbf{b} \rangle$ .

Due to the conservation of total chirality,  $\chi_{\text{tot}} \equiv \langle \mathbf{a} \cdot \mathbf{b} \rangle + 2\langle \mu_5 \rangle / \lambda$ , the generation of small-scale magnetic helicity  $\langle \mathbf{a} \cdot \mathbf{b} \rangle$  causes growth of the mean chiral chemical potential,  $\langle \mu_5 \rangle = -\lambda \langle \mathbf{a} \cdot \mathbf{b} \rangle / 2$ . The small-scale chiral dynamo enhances the turbulent kinetic energy via magnetic driving. The latter increases the fluid and magnetic Reynolds numbers,  $\text{Re} \equiv U_{\text{rms}}/(\nu k_{\text{int}})$  and

TABLE I. Summary of all runs presented in this paper.

Run	$E_5(k, t_0)$	$\mu_{5,\text{rms}}(t_0)$	$\mu_{5,\text{max}}(t_0)$	$\mu_{5,\text{max}}(t_5)$	$\max(\text{Re}_M)$
R-2	$\propto k^{-2}$	13.8	50.5	48.1	288
R-1	$\propto k^{-1}$	15.8	85.8	62.0	134
R+1	$\propto k^1 e^{-(k/10)^2}$	12.6	53.7	53.7	65.1

$\text{Re}_M \equiv U_{\text{rms}}/(\eta k_{\text{int}})$ , where  $k_{\text{int}}^{-1}$  is the integral scale of magnetically-driven turbulence. When  $\text{Re}_M$  is large enough, the mean-field dynamo instability is excited and amplifies a large-scale magnetic field. These theoretical ideas are now checked in DNS.

We use the PENCIL CODE [35] to solve Eqs. (1)–(4) in a 3D periodic domain of size  $L^3 = (2\pi)^3$  with a resolution of  $672^3$ . This code employs a third-order accurate time-stepping method and sixth-order explicit finite differences in space. The smallest wave number covered in the numerical domain is  $k_1 = 2\pi/L = 1$  which we use for normalization of length scales. All velocities are normalized to  $c_s = 1$  and the mean fluid density is  $\bar{\rho} = 1$ . Time is expressed in terms of the magnetic diffusion time  $t_\eta = (\eta k_1^2)^{-1}$  and we use  $\eta = 2 \times 10^{-4}$  in all runs.

For numerical stability, a diffusion of  $\mu_5$  has to be applied in Eq. (4). To affect primarily the largest resolved wave numbers  $k$  in the simulation domain, we use hyperdiffusion, so  $\mathcal{D}_5(\mu_5) = -\mathcal{D}_5 \nabla^4 \mu_5$ ; see the companion paper [36] for technical details. The diffusion constant  $\mathcal{D}_5$  is set to a value that produces the same diffusion rate on the diffusion scale as the one of the magnetic field on the Nyquist scale for the corresponding value of  $\eta$ . Further, the magnetic Prandtl number  $\text{Pr}_M = \nu/\eta$  is 1, i.e.  $\text{Re}_M = \text{Re}$ . These numbers are based on the integral scale of turbulence,

$$k_{\text{int}}^{-1} \equiv \frac{\int_1^{k_{\text{max}}} E_M(k) k^{-1} dk}{\int_1^{k_{\text{max}}} E_M(k) dk}. \quad (5)$$

Here,  $E_M$  is the magnetic energy spectrum as defined by  $\int_0^{k_{\text{max}}} E_M(k, t) dk \equiv \langle \mathbf{B}^2 \rangle / 2$ . Likewise, power spectra of  $\mu_5$  are defined by  $\int_0^{k_{\text{max}}} E_5(k, t) dk \equiv \langle \mu_5^2 \rangle$ . As initial conditions we consider a weak seed magnetic field  $\mathbf{B}$  which has the form of Gaussian noise and a zero velocity field  $\mathbf{U}$ . Initial fluctuations of  $\mu_5$  are also set up as Gaussian noise, but with a specific power spectrum  $E_5$  that follows a power law in  $k$  space, i.e.,  $E_5(t_0) = E_{5,0} (k/k_1)^s \exp(-k^2/k_{\text{cut}}^2)$  with a cutoff  $k_{\text{cut}}$  that is needed for  $s > -1$ . The amplitude  $E_{5,0}$  is chosen such that the maximum value of  $\mu_5$  domain is comparable for all runs at the time  $t_5$ , which marks the onset of the small-scale chiral instability. In all runs, the initial mean value of  $\mu_5$  is vanishing, so that  $\chi_{\text{tot}} = \langle \mathcal{H} \rangle + 2\langle \mu_5 \rangle / \lambda \approx 0$ , and we use  $\lambda = 400$ . An overview of all runs presented in this paper is given in Table I. Run names indicate the slope of the initial  $\mu_5$  spectrum.

In all runs, the presence of fluctuations in  $\mu_5$  results

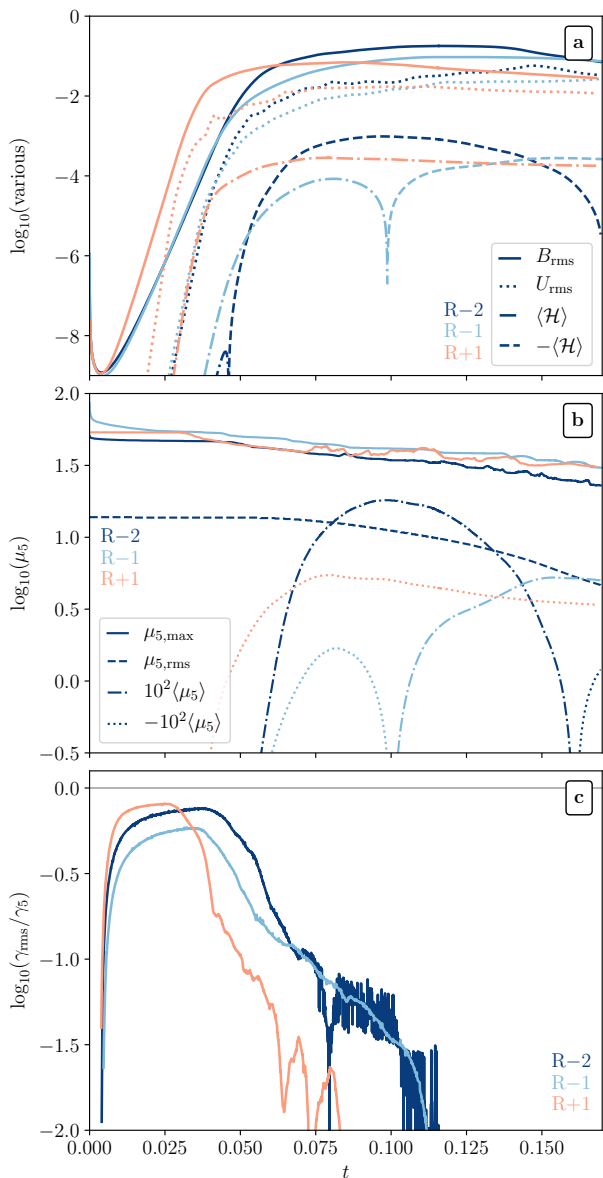


FIG. 1. Direct comparison between the time evolution of different quantities of all simulations. Different colors refer to different runs: R-2 (dark blue), R-1 (light blue), and R+1 (orange). (a) Time series of  $B_{\text{rms}}$ ,  $U_{\text{rms}}$ , and  $\langle \mathcal{H} \rangle$ . (b) Time series of  $\mu_{5,\max}$  and  $\langle \mu_5 \rangle$ . The latter has been multiplied by a factor of 100 for better visualization. (c) Measured growth rate of the rms magnetic field,  $\gamma_{\text{rms}}$ , normalized by  $\gamma_5 = \eta \mu_{5,\max}^2 / 4$ .

in an exponential growth of the rms magnetic field  $B_{\text{rms}}$  at the rate  $\gamma_5$  due to the  $v_5$  dynamo, as can be seen in Fig. 1a. The maximum value of the chiral chemical potential,  $\mu_{5,\max}$ , is larger than  $\mu_{5,\text{rms}}$  by almost an order of magnitude in all runs; see Fig. 1b. Indeed, it is  $\mu_{5,\max}$  which governs the chiral dynamo instability and the usage of  $v_5 = \eta \mu_{5,\max}$  in the expression for the maximum growth rate reproduces the observed growth rate for all runs rather well; see Fig. 1c. We note, however, that a

sufficient separation of scales is required for the dynamo to reach the maximum possible growth rate; see the more detailed analysis in the accompanying paper [36]. During the  $v_5$  dynamo phase, a mean magnetic helicity density  $\langle \mathcal{H} \rangle$  (Fig. 1a) and a mean chiral chemical potential  $\langle \mu_5 \rangle$  (Fig. 1b) are produced. If the divergence of magnetic helicity fluxes is small, the latter two always tend to have opposite signs, as follows from the conservation of the total chirality.

During the  $v_5$  dynamo phase, velocity fluctuations are produced by the Lorentz force,  $(\nabla \times \mathbf{B}) \times \mathbf{B}$ , in Eq. (2). The  $v_5$  dynamo phase ends at  $t \approx 0.03$  for run R+1 and  $t \approx 0.05$  for runs R-2 and R-1 when  $U_{\text{rms}} \approx B_{\text{rms}}$ . In this chiral-magnetically driven turbulence, a large-scale chiral dynamo instability (a mean-field dynamo) can occur if two conditions are satisfied: (i)  $\text{Re}$  and  $\text{Re}_M$  are large and (ii) at the beginning of the nonlinear stage when the inverse cascade starts, the total magnetic helicity  $\langle \mathcal{H} \rangle = \langle \mathbf{A} \rangle \cdot \langle \mathbf{B} \rangle + \langle \mathbf{a} \cdot \mathbf{b} \rangle$  is much smaller than  $2\langle \mu_5 \rangle / \lambda$  to avoid rapid saturation. Turbulence is driven magnetically. Therefore, in particular with the chiral inverse cascade, the turbulent integral scale based on the wave number  $k_{\text{int}}$  changes in time. This is seen in Fig. 2a, which shows the evolution of the magnetic energy spectrum for run R-2. Here, the inverse cascade starts at  $t_{\text{IC}} \approx 0.05$  when the peak of the magnetic energy spectrum reaches  $C_5 \eta^2 \langle \mu_5 \rangle_{\text{int}}(t_{\text{IC}})$  with the constant  $C_5 \approx 16$  [37]. To study the mean-field dynamo, we will perform averages on the scale  $k_{\text{int}}$  (see Fig. 2b), defined as

$$\langle \mu_5 \rangle_{\text{int}} = \left[ \frac{\int_0^{k_{\text{max}}} E_M(k) E_5(k) dk}{\int_0^{k_{\text{max}}} E_M(k) dk} \right]^{1/2}, \quad (6)$$

$$\langle B \rangle_{\text{int}} = \left[ \frac{\int_0^{k_{\text{max}}} E_M(k)^2 dk}{\int_0^{k_{\text{max}}} E_M(k) dk} \right]^{1/2}, \quad (7)$$

$$\langle \mathcal{H} \rangle_{\text{int}} = \frac{\int_0^{k_{\text{max}}} E_M(k) H_M(k) dk}{\int_0^{k_{\text{max}}} E_M(k) dk}, \quad (8)$$

and shown in Fig. 2c.

For magnetically driven turbulence, when the turbulent magnetic energy  $\overline{b^2}$  is much larger than the turbulent kinetic energy  $\overline{u^2}$ , the large-scale dynamo instability is excited by the magnetic  $\alpha$  effect,  $\alpha_M = C_m \tau_c \chi_c$ , where  $\chi_c = \overline{\mathbf{b} \cdot (\nabla \times \mathbf{b})} \approx \langle \mathbf{a} \cdot \mathbf{b} \rangle_{\text{int}} k_{\text{int}}^2$  is the current helicity caused by the magnetic helicity  $\overline{\mathbf{a} \cdot \mathbf{b}}$ ,  $\tau_c = (u_A k_{\text{int}})^{-1}$  is the correlation time of the magnetically driven, weakly inhomogeneous turbulence with the integral scale given by Eq. (5), and the Alfvén speed  $u_A = \sqrt{\overline{b^2}} \approx B_{\text{rms}}$ . Here the overbar denotes ensemble averaging. We recall that the mean fluid density entering in  $u_A$  and  $\alpha_M$  is set to unity. Furthermore,  $C_m = 2(q-1)/(q+1)$  is a coefficient that depends on the exponent  $q$  of the magnetic energy spectrum  $k^{-q}$ . We use  $q = 3$ , see the scaling of  $E_M(k)$  in Fig. 2a. The growth rate of the large-scale dynamo instability for large magnetic Reynolds numbers is

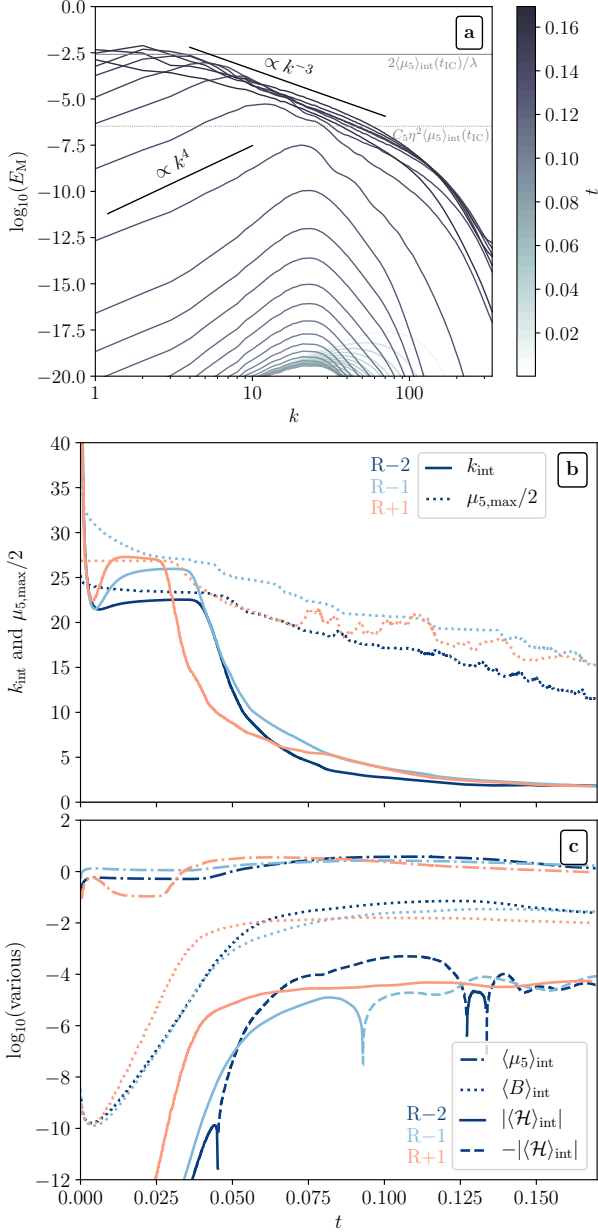


FIG. 2. (a) Time evolution of the magnetic energy spectrum  $E_M$  for run R-2 with time indicated by the colorbar. (b) The wave number based on the integral scale of turbulence,  $k_{\text{int}}$ , as a function of time for all runs (solid lines) and the value of the theoretically predicted wave number,  $\mu_{5,\text{max}}/2$ , on which the  $v_5$  dynamo instability has the largest growth rate (dotted lines). (c) Different averages based on the  $k_{\text{int}}$ :  $\langle \mu_5 \rangle_{\text{int}}$  (dashed-dotted),  $\langle B \rangle_{\text{int}}$  (dotted lines),  $\langle \mathcal{H} \rangle_{\text{int}}$  (solid lines), and  $-\langle \mathcal{H} \rangle_{\text{int}}$  (dashed lines).

given by  $\gamma_{\alpha_M} = |\alpha_M|k - \eta_T k^2$ , where  $\eta_T = u_{\text{rms}}/(3k_{\text{int}})$  is the coefficient of the turbulent magnetic diffusion [14].

With the growth of the magnetic field, the small-scale magnetic helicity  $\overline{\mathbf{a} \cdot \mathbf{b}}$  and the current helicity  $\chi_c$  are evolving. The budget equation for  $\chi_c$  follows from that

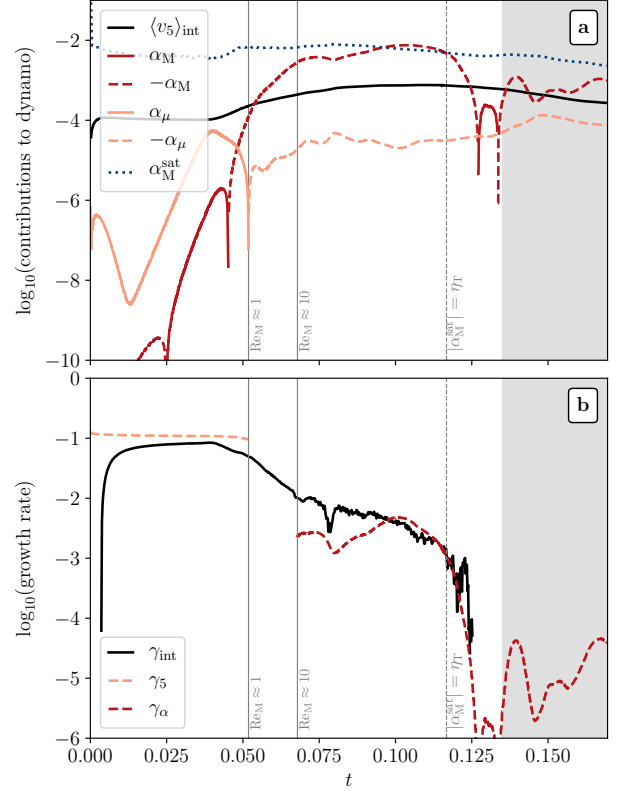


FIG. 3. Time evolution of different quantities in Run R-2. Gray background indicates that the inverse cascade has reached the size of the domain. (a) Different contributions to the mean-field dynamo growth rate, including  $\langle v_5 \rangle_{\text{int}} \equiv \eta \langle \mu_5 \rangle_{\text{int}}$ . (b) The measured growth rate of  $\langle B \rangle_{\text{int}}$ ,  $\gamma_{\text{int}}$  (black solid line) compared to the  $v_5$  dynamo growth rate  $\gamma_5$  (orange dashed line) and the mean-field dynamo growth rate  $\gamma_\alpha$  based on  $\alpha_M$  (red dashed line).

for the magnetic helicity [14]:

$$\frac{\partial}{\partial t} \overline{\mathbf{a} \cdot \mathbf{b}} + \text{div } \mathbf{F} = 2\overline{v_5 \mathbf{b}^2} - 2\overline{\boldsymbol{\mathcal{E}} \cdot \mathbf{B}} - 2\eta_T \overline{\mathbf{b} \cdot (\nabla \times \mathbf{b})}, \quad (9)$$

where  $\mathbf{F}$  is the flux of  $\overline{\mathbf{a} \cdot \mathbf{b}}$  and  $\boldsymbol{\mathcal{E}} \equiv \overline{\mathbf{u} \times \mathbf{b}} = \alpha_M \overline{\mathbf{B}} - \eta_T (\nabla \times \overline{\mathbf{B}})$  is the electromotive force. Here we consider the case when the kinetic  $\alpha$  effect caused by the kinetic helicity and the chiral  $\alpha_\mu$  effect [14] are much smaller than the magnetic  $\alpha$  effect. This is a typical situation for the chiral mean-field dynamo with nonuniform  $\mu_5$ . In saturation, two leading source/sink terms in Eq. (9),  $2\overline{v_5 \mathbf{b}^2} - 2\alpha_M \overline{\mathbf{B}^2}$ , compensate each other, so that the magnetic  $\alpha$  effect reaches the value

$$\alpha_M^{\text{sat}} = \eta \overline{\mu_5} \frac{\overline{\mathbf{b}^2}}{\overline{\mathbf{B}^2}}. \quad (10)$$

For R-2,  $|\alpha_M|$  dominates once turbulence sets in and  $|\alpha_M| \approx |\alpha_M^{\text{sat}}|$  for  $t \gtrsim 0.075$ , as can be seen in Fig. 3a.

The maximum growth rate of the chiral mean-field dynamo instability is given by  $\gamma_\alpha = \alpha_M^2/(4\eta_T)$  and agrees well with the measured growth rate of  $\langle B \rangle_{\text{int}}$ ,  $\gamma_{\text{int}}$ ; see

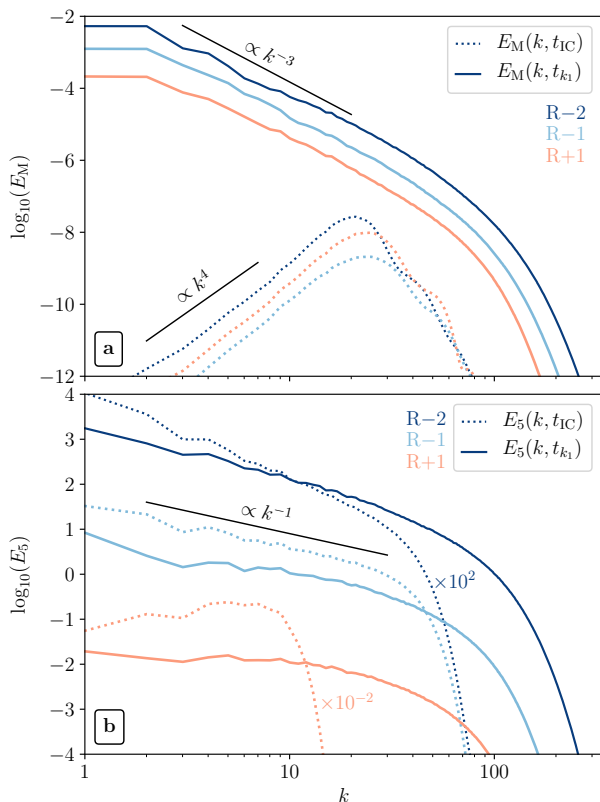


FIG. 4. Power spectra from all simulations. (a) Magnetic energy spectra  $E_M$  at the beginning of the chiral inverse cascade  $t_{IC}$  (dotted lines) and the time when the cascade reaches the size of the numerical domain  $t_{k_1}$  (solid lines). (b) Spectra of  $\mu_5$  shown at the same two characteristic times as  $E_M$ . For better visibility the spectra of runs R-2 and R+1 have been multiplied by factors of  $10^2$  and  $10^{-2}$ , respectively.

Fig. 3b for run R-2 in the interval  $0.075 < t < 0.12$ . In our DNS, the measured growth rate  $\gamma_{\text{int}}$  of the mean-field dynamo strongly decreases when the scale at which  $\gamma_\alpha$  is maximum becomes larger than the size of the box. As can be seen in Fig. 3b,  $\gamma_{\text{int}}$  vanishes once the positive contribution to the growth rate on the minimum wave number of the box,  $|\alpha_M^{\text{sat}}|k_1$ , becomes comparable to the negative contribution,  $\eta_T k_1^2$ . For R-2, dissipation on the box scale dominates for  $t \gtrsim 0.12$ .

After saturation we observe the formation of universal power spectra of  $\mu_5$  in all of the runs; see Fig. 4. All of the  $\mu_5$  spectra approach a  $k^{-1}$  scaling at the time  $t_{k_1}$  when the peak of the magnetic energy reaches the size of the domain. The magnetic energy spectra approach a  $k^{-3}$  scaling which is, for fully helical magnetic fields, consistent with the magnetic helicity spectra that approach a scaling  $\propto k^{-4}$ .

In conclusion, a small-scale chiral dynamo can arise from an initially fluctuating chiral chemical potential with zero mean. The chiral dynamo generates small-scale magnetic helicity which (i) causes the production of a mean  $\mu_5$  due to the conservation of total chirality

and (ii) drives turbulence via the Lorentz force. In our DNS, sufficiently strong turbulence is generated to activate a mean-field dynamo that is well described by the magnetic  $\alpha$  effect caused by current helicity. The latter is generated by the source term  $2\bar{v}_5 \bar{\mathbf{b}}^2$  originating from magnetic fluctuations produced by inhomogeneous fluctuations of  $\mu_5$ . During the mean-field dynamo phase, the power spectra develop a universal shape;  $E_M \propto k^{-3}$  and  $E_5 \propto k^{-1}$ . In particular, with the onset of turbulence in the system,  $\mu_5$  becomes scale-invariant, independent of its initial condition.

We have benefited from stimulating discussions with Nathan Kleorin and Abhijit B. Bendre. JS acknowledges the support by the Swiss National Science Foundation under Grant No. 185863. AB was supported in part through a grant from the Swedish Research Council (Vetenskapsrådet, 2019-04234).

\* jennifer.schober@epfl.ch

- [1] A. Vilenkin, Equilibrium parity violating current in a magnetic field, *Phys. Rev. D* **22**, 3080 (1980).
- [2] D. E. Kharzeev, The chiral magnetic effect and anomaly-induced transport, *Prog. Part. Nucl. Phys.* **75**, 133 (2014).
- [3] D. E. Kharzeev, J. Liao, S. A. Voloshin, and G. Wang, Chiral magnetic and vortical effects in high-energy nuclear collisions-A status report, *Progress in Particle and Nuclear Physics* **88**, 1 (2016).
- [4] A. Boyarsky, J. Fröhlich, and O. Ruchayskiy, Self-Consistent Evolution of Magnetic Fields and Chiral Asymmetry in the Early Universe, *Phys. Rev. Lett.* **108**, 031301 (2012).
- [5] D. J. Schwarz and M. Stuke, Lepton asymmetry and the cosmic QCD transition, *J. Cosmol. Astropart. Phys.* **11**, 025 (2009).
- [6] A. Brandenburg, Y. He, T. Kahniashvili, M. Rheinhardt, and J. Schober, Relic Gravitational Waves from the Chiral Magnetic Effect, *Astrophys. J.* **911**, 110 (2021).
- [7] D. G. Figueroa, A. Florio, and M. Shaposhnikov, Chiral charge dynamics in Abelian gauge theories at finite temperature, *Journal of High Energy Physics* **2019**, 142 (2019).
- [8] M. Mace, N. Mueller, S. Schlichting, and S. Sharma, Chiral Instabilities and the Onset of Chiral Turbulence in QED Plasmas, *Phys. Rev. Lett.* **124**, 191604 (2020).
- [9] M. A. Stephanov and Y. Yin, Chiral Kinetic Theory, *Phys. Rev. Lett.* **109**, 162001 (2012).
- [10] J.-Y. Chen, D. T. Son, and M. A. Stephanov, Collisions in chiral kinetic theory, *Phys. Rev. Lett.* **115**, 021601 (2015).
- [11] E. V. Gorbar, I. A. Shovkovy, S. Vilchinskii, I. Rudenok, A. Boyarsky, and O. Ruchayskiy, Anomalous maxwell equations for inhomogeneous chiral plasma, *Physical Review D* **93**, 105028 (2016).
- [12] N. Yamamoto and D.-L. Yang, Chiral Radiation Transport Theory of Neutrinos, *Astrophys. J.* **895**, 56 (2020).
- [13] M. Giovannini, Anomalous magnetohydrodynamics, *Phys. Rev. D* **88**, 063536 (2013).

- [14] I. Rogachevskii, O. Ruchayskiy, A. Boyarsky, J. Fröhlich, N. Kleeorin, A. Brandenburg, and J. Schober, Laminar and turbulent dynamos in chiral magnetohydrodynamics I: Theory, *Astrophys. J.* **846**, 153 (2017).
- [15] L. Del Zanna and N. Bucciantini, Covariant and 3+ 1 equations for dynamo-chiral general relativistic magnetohydrodynamics, *Monthly Not. Roy. Astron. Soc.* **479**, 657 (2018).
- [16] K. Hattori, Y. Hirono, H.-U. Yee, and Y. Yin, Magnetohydrodynamics with chiral anomaly: Phases of collective excitations and instabilities, *Phys. Rev. D* **100**, 065023 (2019).
- [17] M. Joyce and M. Shaposhnikov, Primordial Magnetic Fields, Right Electrons, and the Abelian Anomaly, *Phys. Rev. Lett.* **79**, 1193 (1997).
- [18] J. Schober, I. Rogachevskii, A. Brandenburg, A. Boyarsky, J. Fröhlich, O. Ruchayskiy, and N. Kleeorin, Laminar and Turbulent Dynamos in Chiral Magnetohydrodynamics II. Simulations, *Astrophys. J.* **858**, 124 (2018).
- [19] J. Schober, A. Brandenburg, I. Rogachevskii, and N. Kleeorin, Energetics of turbulence generated by chiral mhd dynamos, *Geophys. Astrophys. Fluid Dyn.* **113**, 107 (2019).
- [20] J. Schober, A. Brandenburg, and I. Rogachevskii, Chiral fermion asymmetry in high-energy plasma simulations, *Geophys. Astrophys. Fluid Dyn.* **114**, 106 (2020).
- [21] Y. Hirono, D. E. Kharzeev, and Y. Yin, Self-similar inverse cascade of magnetic helicity driven by the chiral anomaly, *Phys. Rev. D* **92**, 125031 (2015).
- [22] E. V. Gorbar, I. Rudenok, I. A. Shovkovy, and S. Vilchinskii, Anomaly-driven inverse cascade and inhomogeneities in a magnetized chiral plasma in the early universe, *Phys. Rev. D* **94**, 103528 (2016).
- [23] K. Subramanian, The origin, evolution and signatures of primordial magnetic fields, *Rep. Prog. Phys.* **79**, 076901 (2016).
- [24] T. Vachaspati, Progress on cosmological magnetic fields, *Reports on Progress in Physics* **84**, 074901 (2021).
- [25] A. Neronov and I. Vovk, Evidence for Strong Extragalactic Magnetic Fields from Fermi Observations of TeV Blazars, *Science* **328**, 73 (2010).
- [26] M. Dvornikov and V. B. Semikoz, Magnetic helicity evolution in a neutron star accounting for the adler-bell-jackiw anomaly, *J. Cosmol. Astropart. Phys.* **2018** (08), 021.
- [27] Y. Masada, K. Kotake, T. Takiwaki, and N. Yamamoto, Chiral magnetohydrodynamic turbulence in core-collapse supernovae, *Phys. Rev. D* **98**, 083018 (2018).
- [28] N. Yamamoto, Chiral transport of neutrinos in supernovae: Neutrino-induced fluid helicity and helical plasma instability, *Phys. Rev. D* **93**, 065017 (2016), arXiv:1511.00933 [astro-ph.HE].
- [29] G. Sigl and N. Leite, Chiral Magnetic Effect in Protoneutron Stars and Magnetic Field Spectral Evolution, *JCAP* **1601** (01), 025, arXiv:1507.04983 [astro-ph.HE].
- [30] G. Sigl and N. Leite, Chiral magnetic effect in protoneutron stars and magnetic field spectral evolution, *JCAP* **1**, 025.
- [31] M. Dvornikov, V. B. Semikoz, and D. D. Sokoloff, Generation of strong magnetic fields in a nascent neutron star accounting for the chiral magnetic effect, *Phys. Rev. D* **101**, 083009 (2020).
- [32] Y. Hirono, D. E. Kharzeev, and Y. Yin, New quantum effects in relativistic magnetohydrodynamics, *Nuclear Phys. A* **967**, 840 (2017).
- [33] V. Galitski, M. Kargarian, and S. Syzranov, Dynamo Effect and Turbulence in Hydrodynamic Weyl Metals, *Phys. Rev. Lett.* **121**, 176603 (2018).
- [34] D. E. Kharzeev and H.-U. Yee, Chiral magnetic wave, *Phys. Rev. D* **83**, 085007 (2011).
- [35] Pencil Code Collaboration, A. Brandenburg, A. Johansen, P. Bourdin, W. Dobler, W. Lyra, M. Rheinhardt, S. Bingert, N. Haugen, A. Mee, F. Gent, N. Babkovskaia, C.-C. Yang, T. Heinemann, B. Dintrans, D. Mitra, S. Candelaresi, J. Warnecke, P. Käpylä, A. Schreiber, P. Chatterjee, M. Käpylä, X.-Y. Li, J. Krüger, J. Aarnes, G. Sarson, J. Oishi, J. Schober, R. Plasson, C. Sandin, E. Karchniwy, L. Rodrigues, A. Hubbard, G. Guerrero, A. Snodin, I. Losada, J. Pekkila, and C. Qian, The Pencil Code, a modular MPI code for partial differential equations and particles: multipurpose and multiuser-maintained, *The Journal of Open Source Software* **6**, 2807 (2021).
- [36] J. Schober, I. Rogachevskii, and A. Brandenburg, Dynamo instabilities in plasmas with inhomogeneous chiral chemical potential, companion Paper.
- [37] A. Brandenburg, J. Schober, I. Rogachevskii, T. Kahnishvili, A. Boyarsky, J. Fröhlich, O. Ruchayskiy, and N. Kleeorin, The turbulent chiral-magnetic cascade in the early universe, *Astrophys. J. Lett.* **845**, L21 (2017).